Geomechanics and Engineering, *Vol. 6, No. 2 (2014) 153-172*
DOI: http://dx.doi.org/10.12989/gae.2014.6.2.153

Hydraulic fracturing experiments of highly deviated well with oriented perforation technique

Hai Y. Zhu [*1,2], Jin G. Deng [2a], Shu J. Liu [3], Min Wen [3], Cheng Y. Peng [3], Ji R. Li [2], Zi J. Chen [2], Lian B. Hu [2], Hai Lin [2] and Dong Guang [4]

[1] *State Key Laboratory of Oil & Gas Reservoir Geology and Exploitation, Southwest Petroleum University, Chengdu 610500, China*
[2] *State Key Laboratory of Petroleum Resource and Prospecting (China University of Petroleum, Beijing), Beijing 102249, China*
[3] *CNOOC Research Institute, Beijing 100027, China*
[4] *Research Institute of Engineering and Technique, Huabei Sub-Company, SINOPEC, Zhengzhou, Henan 450006, China*

(*Received July 08, 2013, Revised September 02, 2013, Accepted September 22, 2013*)

Abstract. In order to investigate the effect of different perforation angles (the angle between the perforation direction and the maximum horizontal principal stress) on the fracture initiation and propagation during hydraulic fracturing of highly deviated well in oil & gas saturated formation, laboratory experiments of the hydraulic fracturing had been carried out on the basis of non-dimensional similar criteria by using 400^3 mm^3 cement cubes. A plane fracture can be produced when the perforations are placed in the direction of the maximum horizontal principal stress. When the perforation angle is 45°, the fractures firstly initiate from the perforations at the upper side of the wellbore, and then turn to the maximum horizontal principal stress direction. When the well deviation angle and perforation angle are both between 45° and 90°, the fractures hardly initiate from the perforations at the lower side of the wellbore. Well azimuth (the angle between the wellbore axis and the maximum horizontal principal stress) has a little influence on the fracture geometries; however it mainly increases the fracture roughness, fracture continuity and the number of secondary fractures, and also increases the fracture initiation and propagation pressure. Oriented perforating technology should be applied in highly deviated well to obtain a single plane fracture. If the well deviation angle is smaller, the fractures may link up.

Keywords: oriented perforating; highly deviated well; hydraulic fracturing; fracture initiation; fracture propagation

1. Introduction

Hydraulic fracturing is now widely used to stimulate oil production in the unconventional oil and gas formations with low permeability that was inaccessible before. The sand or other proppants are left in the fracture after hydraulic fracturing, holding the fractures open to allow the

*Corresponding author, Ph.D., E-mail: zhuhaiyan040129@163.com
[a] Professor, E-mail: dengjingen@126.com

http://www.techno-press.org/?journal=gae&subpage=7 ISSN: 2005-307X (Print), 2092-6219 (Online)

oil to flow freely out of the formation and into a production well. Field applications indicate that most hydraulic fracturing works are operated in cased well with perforating completion technique, and the perforation tunnels are the flow paths of the fracturing fluid between the hydraulic fractures and wellbore (Abass *et al*. 1994, Mahrer *et al*. 1996). Many scholars (Daneshy 1973a, b, King 1989, Behrmaan and Elbel 1991, Hallam and Last 1991, Pearson *et al*. 1992, Soliman *et al*. 2008) have proposed that hydraulic fracturing can produce a large plane fracture when the perforations perfectly align with the preferred fracture plane (PFP), namely the perforation angle is 180° or 0°. When the perforations don't align with the PFP, the fracture geometries may be complicated. The greater the perforation angle is, the higher the fracture initiation pressure is, and the more complicated the fracture geometries are.

It is difficult to directly observe the fracture initiation and propagation. Some analytical models are used to simulate hydraulic fracturing problem indirectly based on various assumptions and simplified conditions, such as PKN (Nordgren 1972), GDK (Khristianovic and Zheltov 1955), radial Penny model (Sneddon and Elliot 1946), PL3D (Siebrits and Peirce 2002) and P3D (Mack and Warpinski 2000) model. In recent years, some numerical calculation methods including finite element method (Cao and Liu 2012, Liao *et al*. 2012, Akhaveissy *et al*. 2013), finite difference method (Nagel and Sanchez-Nagel 2011), the boundary element method (BEM) (Rahman *et al*. 2002, Hossain and Rahman 2008), displacement discontinuity method (DDM) (Zhang *et al*. 2007, 2009) and the discrete element method (DEM) (Nagel and Sanchez-Nagel 2012) are used to calculated initiation and propagation of hydraulic fractures. The existing computing softwares for hydraulic fracturing are: FLAC3D (Nagel and Sanchez-Nagel 2011), FRANC3D (Rahman *et al*. 2002), HYFRANC3D (Hossain and Rahman 2008), RFPA (Tang *et al*. 2002), Abaqus (Chen *et al*. 2009, Zhang *et al*. 2010), UDEC/3DEC (Nagel and Sanchez-Nagel 2011, 2012) and so on. Although numerical calculation methods are effective to solve the fracture initiation and propagation problems of some vertical, horizontal and medium deviated wells, for highly deviated well with perforations of different phases it is hard to solve the high nonlinear problem caused by its complex fractures.

Hydraulic fracturing experiment which considers the formation conditions is an important way to understand the mechanism of hydraulic fracture initiation and propagation. Hydraulic fractures can be monitored and observed by the experiment directly. Table 1 summarizes the test parameters of typical laboratory hydraulic fracturing experiments since the 1970s, where σ_v, σ_H and σ_h are the vertical stress, the maximum horizontal principle stress and the minimum horizontal stress respectively. We can find that the studies about the initiation and propagation mechanism of the hydraulic fracture are mostly proposed between the 1970s and 1990s. The cement and cement-sand mixture are used to simulate the formation rock. Rock samples are mainly 152 × 152 × 254 mm^3 for vertical or horizontal well hydraulic fracturing experiments and 300^3 mm^3 for deviated well. The viscosity of the test liquid is between 0.03-1.3, which is similar to the field condition. However, according to the scaling analysis by De Pater *et al*. (1994), a very high viscosity must be used to properly scale to the field condition (because of the orders of magnitude lower flow rate). Also, few systematic researches on hydraulic fracturing with oriented perforations and different well azimuth and deviation angles of highly deviated well have been done. In this paper, using 400^3 mm^3 cement-sand samples, laboratory hydraulic fracturing experiments are carried out. The influences of oriented perforating on the fracture initiation and propagation of highly deviated well with different well deviation, well azimuth and perforation angles are further studied. The fracture initiation and propagation mechanism of highly deviated well are found out to provide the theoretical guidance for hydraulic fracturing treatment.

Table 1 Test parameters in the hydraulic fracturing experiments

Parameters	Daneshy	Daneshy	Ahmed *et al.*	EI Rabaa	Hallam and Last	Kim and Abass	Abass	Weijers and De Pater	Brumley and Abass	Van de Ketterij and De Pater	Deng *et al.*	Jiang *et al.*
Time	1973a	1973b	1983	1989	1991	1991	1992	1992	1996	1997	2008	2009
Sample ingredients	Water, cement	Limestone or cement	Cement	Cement	Cement, silica sand powder	Cement	Cement	Cement and fine sand	Cement	Cement and fine sand	Cement and sand	Cement and fine sand
Mix ratio of water to cement or sand	0.35	0.35		0.35	9/1/3	0.32	0.32	1/0.43	0.32	27/23	3/1	1/1
Size mm	150×150×250	150×150×250	1000^3	150×300×450	300^3	150×150×250	150×150×250	300^3	150×150×250	300^3	300^3	300^3
Borehole diameter mm	8	8	3.2	8	6.4	19	19	20	76.2	20	20	20
Casing inner diameter mm	6	Open hole		Open hole	4.8	16	16	19.5	Open hole	8	8	15
Perforations /per rank	10, 6, 5, 3, 2, 1		15			7	7	1、9		9	2-4	3
Perforation diameter mm	3.2		1		0.4	2.4	2.4	3		3	4	2
Perforation length mm	3.2				7	20.8	20.8	25		25	20	30
Perforation space mm	20-30				9.4	10.4	10.4	12.5		12.5/50		
σ_v MPa	7	7	13.8	51.7	14	20.7	20.7	23	20.7	23	13	15
σ_H MPa	5.5	5.5	13.1	50.3	14	17.2	17.2	12.1	17.2	12.1-19.4	11	4-6
σ_h MPa	3.5	3.5	8.3	38.5	4.8	9.7	9.7	9.7	9.7	9.7	9	1
Inclination	Vertical	8, 16, 24	Vertical	Horizontal	0, 10, 20, 30	Horizontal	Horizontal	45/49	0, 22.5, 45, 67.5, 90	49	0, 30	Vertical
Azimuth	30, 60, 90	0-75°		0-90	0-90	0-90	0-90	30, 60	0-90	60	0-90	0-75
Phase azimuth	0, 180, spiral	0, 180			180	180	180	0, 180		0, 90, 180	180	180
Test liquid			Fracturing liquid	10# heavy engine oil	Lubricating oil	30# heavy oil	30# engine oil	100# oil	Fracturing liquid	Fracturing liquid	Heavy hydraulic fluid	Guanidine gum liquid
Viscosity Pa.s			0.030-0.3	0.36-0.58	6.5	0.36-0.58	0.36-0.58	0.3	1.3	0.1/0.5	0.1	0.073
Injection rate cm^3/min	136.2	136.2, 1020-1380	204-582	84-333	10	40	30	0.2-1	10	0.088-0.44		0.126

2. Design of laboratory hydraulic fracturing experiments with oriented perforating technique

2.1 Field conditions scaling

The size limitation of the laboratory experiment equipments makes it impossible to simulate the full-scale test of hydraulic fracturing, so the numerical scaling for experimental rock, perforation tunnel, injection rate and the fracture fluid property is necessary. De Pater *et al.* (1994) introduced a scale model for the laboratory experiment based on the theoretical analysis and the laboratory experiment. Bunger *et al.* (2005) introduced a laboratory experiment design scale for the penny-shaped fracture. Using a pseudo three-dimensional model of hydraulic fracturing established by Clifton and Abou-Sayed (1979), Liu *et al.* (2000) gave a similarity principle for the laboratory experiment. Their similarity groups and the groups' theoretical origins are presented in the Appendix. For the parameters of the Z1-C5 well in the Southeast China Sea area, the experimental parameters obtained by the similarity principle are listed in Table 2. The confining

Table 2 Basic experimental parameters

Parameter	Experimental parameters	Field parameter
Wellbore size (mm)	18	177.8 (7 in)
Perforation interval (mm)	20	200
Perforation row	3	3
Perforation diameter (mm)	2	>= 9
Perforation length (mm)	60	>= 300
Injection rate (cm^3/min)	0.126	2000000
Viscosity of fracture fluid (Pa·s)	2.4	0.04-0.6

Fig. 1 400^3 mm^3 true tri-axial hydraulic fracturing test equipment

pressures of the text samples are the same with the in-situ stresses of this oilfield which are 58.2 MPa (the vertical stress), 54.6 MPa (the max. horizontal stress) and 42.5 MPa (the min. horizontal stress) respectively.

2.2 Experimental equipments

The hydraulic fracturing experiment was carried on the 400^3 mm^3 tri-axial hydraulic fracturing test equipment (Fig. 1) (Zhu *et al*. 2013). The horizontal principal stresses and vertical stress are generated by four hydraulic jacks at the outside of the sample and a hydraulic jack below the sample respectively. The maximum pressure of the hydraulic jack is 60 MPa. Using the MTS servo booster pump, the high-pressure liquid is pumped into the simulation borehole in this experiment (Zhu *et al*. 2012). The pressure is observed and recorded by MTS data acquisition system during the experiment. More detail information about the schematic diagram of tri-axial hydraulic fracturing test system can be seen in the paper published by Zhou *et al*. (2010).

2.3 Scheme design

We respectively simulate wellbores of 0°, 30°, 45° and 60° deviation angles with different perforation angles and well azimuth angles (Table 3). Fig. 2 illustrates the rock sample size and the location of the perforation tunnels. We use the concrete made by cement and fine-sand with proportion of 1:1 to simulate the formation rock. The elastic modulus of the concrete is 8.4 GPa, the Poisson's ratio is 0.23, the tensile strength is 3.1 MPa, the UCS is 29.2 MPa, the permeability is 0.2 mD, and the porosity is 2.32%. A special mold which consists of one bottom plate and four side plates is designed to make a 400^3 mm^3 rock sample (Fig. 3). The simulated wellbore is a steel pipe with 18 mm outer diameter, and 8 mm inner diameter. Three holes of 2 mm diameter are drilled at 20 mm over the bottom of the steel pipe, and some plastic pipes which simulate 60 mm

Table 3 Experiment schemes

No.	Injection rate L/min	Deviation °	Azimuth °	Perforation angle °	Perforation length mm	Side distance mm	Top distance mm	Bottom distance mm
1	0.126	45	0	0	0	153	184	188
2	0.126	45	0	0	60	110	142	145
3	0.126	45	0	45	60	110	142	145
4	0.126	45	0	90	60	110	142	145
5	0.126	45	45	0	60	110	142	145
6	0.126	45	45	45	60	110	142	145
7	0.126	45	45	90	60	110	142	145
8	0.126	45	90	0	60	110	142	145
9	0.126	45	90	45	60	110	142	145
10	0.126	45	90	90	60	110	142	145
11	0.126	30	45	45	60	113	157	148
12	0.126	60	45	45	60	113	128	148

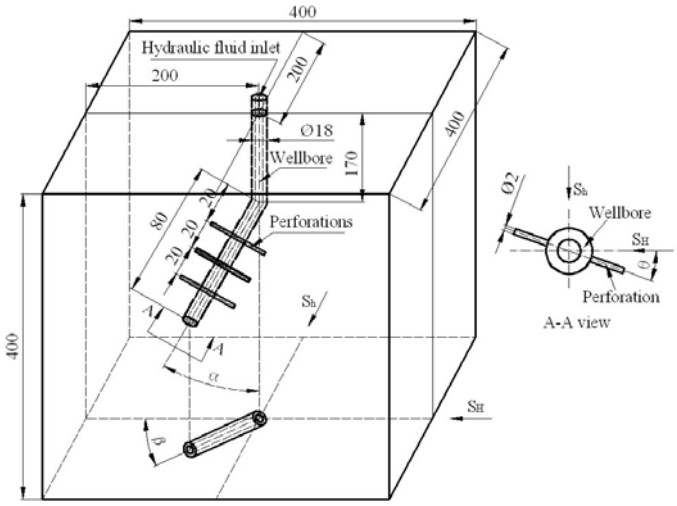

Fig. 2 Size of the sample and the perforation location

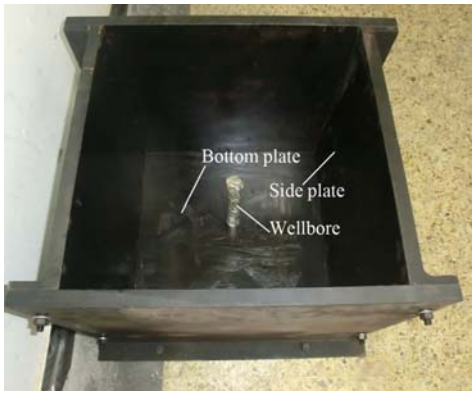

Fig. 3 Rock sample mold and simulated wellbore

pre-set perforation tunnels are inserted into these holes. Pour the concrete into the mold and stir the concrete enough to release the air contained in the concrete. Finally, keep the concrete in a 28°C room for a month and then remove it out.

3. Experimental results and discussions

3.1 Fracture initiation and propagation pressure

When the well deviation angle is 45°, and the well azimuth angles are 0°, 45° and 90° respectively, the fracture initiation pressure increases with the increasing of the perforation angle (Fig. 4). When the perforation angles are 45° and 90°, the fracture initiation pressure and

propagation pressure increase with the well azimuth angles. When the perforation angle is 0°, the fracture initiation pressure and propagation pressure increase at first and then decrease with the well azimuth angle increasing, that means that the fracture initiation pressure and propagation pressure are the largest when the well azimuth angle is 45°. Fig. 5 illustrates that the fracture initiation and propagation pressure increase rapidly with the increasing of the well deviation angles.

3.2 Fracture geometries with different perforation angles

3.2.1 Fracture geometries with 45° well deviation and 0° perforation

Whatever the well azimuth is, a big plane fracture can be produced (Fig. 6). The fractures are all tensile (I) type cracks, and all initiate from the perforation tunnels in the PFP. When the well azimuths are 0° and 90°, a smooth plane fracture initiates (Figs. 6 (a), (c)). When the well azimuth

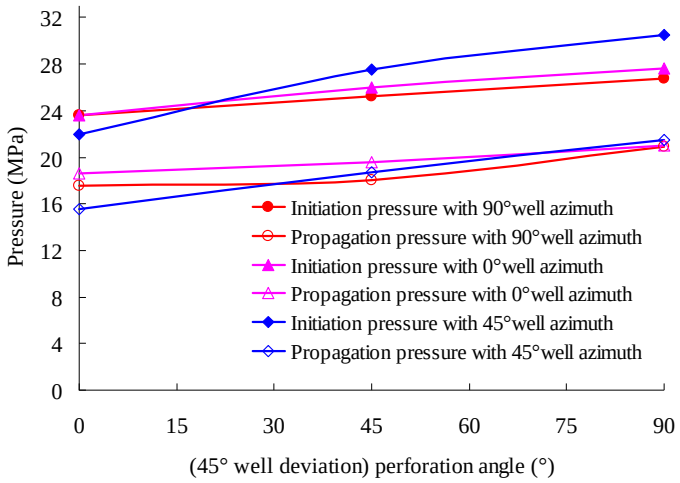

Fig. 4 Fracture initiation and propagation pressure with different perforation angles

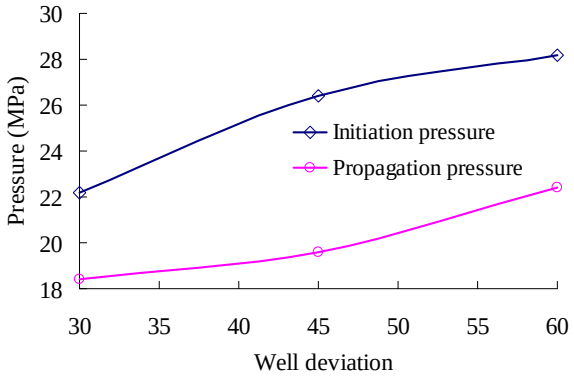

Fig. 5 Fracture initiation and propagation pressure with different well deviation angles

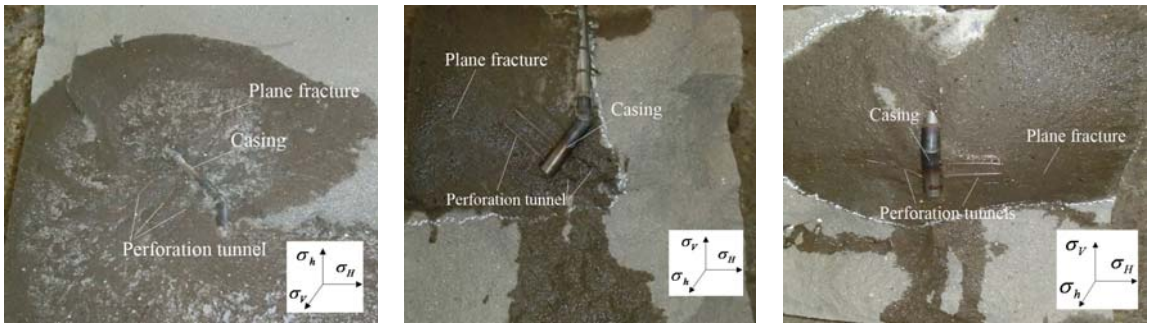

(a) 0° well azimuth (b) 45° well azimuth (c) 90° well azimuth

Fig. 6 Fracture geometries with 0° perforation angle

is 45°, the fracture initiates in the PFP and propagates at the upper part of the wellbore (Fig. 6(b)). Secondary fracture occurs and the surface of the plane fracture is rough, which can explain why the initiation pressure and propagation pressure are higher than what of the 0° and 90° well azimuths. What should be noticed is that when the well azimuth is 45°, though the fracture initiates at both sides of the perforations, it doesn't propagate further at the lower side of the wellbore.

3.2.2 Fracture geometries with 45° well deviation and 45° perforation

The fractures are mainly tensile (I) type and shear (II) type cracks, shear (II) type cracks are mainly turning fractures (Fig. 7). The fracture geometries are very complicated, including plane fractures, turning fractures, parallel fractures, secondary fractures and discontinuous fractures etc. The propagation model for arbitrary fractures in oriented perforations is shown in Fig. 8 (Zhang *et al*. 2008, Zhu *et al*. 2012). The stress intensity factors of the fracture tip can be expressed as (Zhou *et al*. 2010, Kim *et al*. 2012)

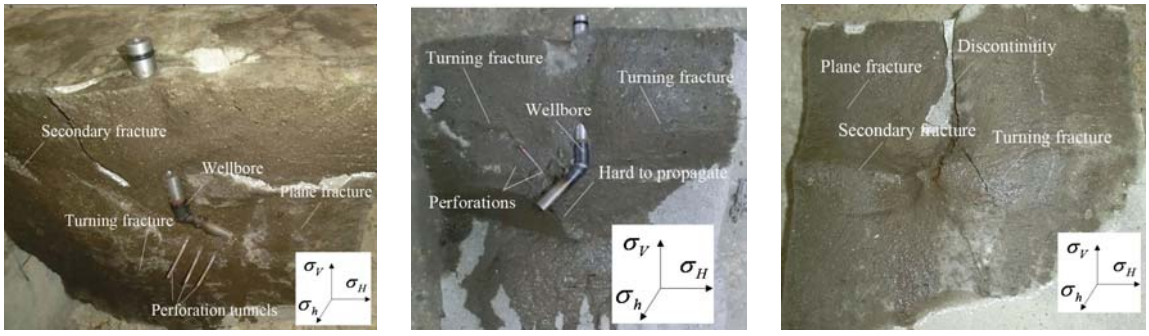

(a) 0° well azimuth (b) 45° well azimuth (c) 90° well azimuth

Fig. 7 Fracture geometries with 45° perforation angle

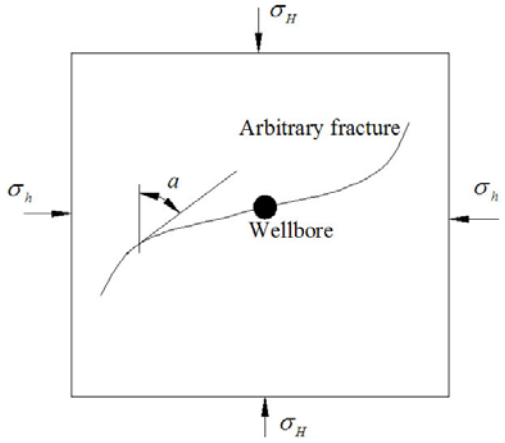

Fig. 8 Propagation model for arbitrary fractures in oriented perforation

$$\begin{cases} K_{\mathrm{I}} = \dfrac{1}{\sqrt{\pi s}}\displaystyle\int_s \left[p(x)\sqrt{\dfrac{s+x}{s-x}} \right] dx - \dfrac{(\sigma_H + \sigma_h)\sqrt{\pi s}}{2} + \dfrac{\sigma_H - \sigma_h}{2\sqrt{\pi s}} \int_s \left[\sqrt{\dfrac{s+x}{s-x}} \cos 2\alpha \right] dx \\ K_{\mathrm{II}} = \dfrac{\sigma_H - \sigma_h}{2\sqrt{\pi s}} \displaystyle\int_s \left[\sqrt{\dfrac{s+x}{s-x}} \sin 2\alpha \right] dx \end{cases} \tag{1}$$

Circumferential stress of the fracture tip

$$\sigma_\theta = \frac{K_{\mathrm{I}}}{2\sqrt{\pi r}} \cos^3 \frac{\theta}{2} - \frac{3K_{\mathrm{II}}}{2\sqrt{\pi r}} \sin \frac{\theta}{2} \cos^2 \frac{\theta}{2} \tag{2}$$

Criterion of fracture propagation

$$K_{\mathrm{I}} \geq K_{\mathrm{IC}}, \quad K_{\mathrm{II}} \geq K_{\mathrm{IIC}} \tag{3}$$

Fracture propagation direction

$$\theta = \arccos\left(\frac{3K_{\mathrm{II}}{}^2 + K_{\mathrm{I}}\sqrt{K_{\mathrm{I}}{}^2 + 8K_{\mathrm{II}}{}^2}}{K_{\mathrm{I}}{}^2 + 9K_{\mathrm{II}}{}^2} \right) \tag{4}$$

where, $p(x)$ is the net pressure acting on the fracture surface, s is the fracture trajectory, a is the fracture length, x is the distance between a point on fracture and the wellbore. The fracture turning position and direction can be calculated using above equations.

When the well azimuth is 0°, the fracture initiates along the perforations at the lower side, turns to the PFP and form a turning fracture; a big plane fracture is created at the upper side of deviated wellbore; also a secondary fracture occurs (Fig. 7(a)). When the well azimuth is 45°, the fracture initiates along the perforations at the upper side and forms a turning fracture; the fracture at the

lower side initiates along the perforations and do not propagate further (Fig. 7(b)). When the well azimuth is 90°, the fracture initiates along the perforations at the upper side and forms a turning fracture; although the fracture initiates alone the lower side perforations, it is hard to propagate; a plane fracture is also created at the upper side of deviated wellbore; there is a discontinuous fracture around the vertical borehole (Fig. 7(c)).

3.2.3 Fracture geometries with 45° well deviation and 90° perforation

When the well azimuths are 0° and 45°, twist (III) type cracks are produced (Fig. 9). For a circular fracture, if its radius is *a*, the stress intensity factors of the fracture tip can be expressed as (Luo *et al*. 2012)

$$K_{\mathrm{I}} = \frac{2}{\sqrt{\pi}} p(x)\sqrt{\pi a}, \quad K_{\mathrm{III}} = \frac{4}{3\pi}\tau\sqrt{\pi a} \tag{5}$$

The fracture twist angle (Alshoaibi 2010)

$$\Phi = \frac{1}{2} a \tan\left[\frac{2K_{\mathrm{III}}}{K_{\mathrm{I}}(1-2v)}\right] \tag{6}$$

As illustrated in Fig. 9(a), when the well azimuth is 0°, a horizontal fracture is produced; in the maximum horizontal principle stress direction, some branched fractures are created; the fractures are hard to initiate from the perforations of the second and third rows. When the well azimuth is 45°, the fracture geometry is similar to the fracture of 0° well azimuth; the hydraulic fracture only initiates from the perforations of the first row; the fracture surface is very rough, some secondary fractures and discontinuous are produced (Fig. 9(b)). When the well azimuth is 90°, the fracture initiates from the perforations at the upper side of the wellbore, and then twists to maximum horizontal principle stress direction; there are no fractures initiated from the perforations at the lower side of the wellbore (Fig. 9(c)). When the perforation angle is 90°, whatever the well deviation and azimuth angle are, the hydraulic fracture geometries are very complicated, the fractures are hard to initiate from the perforations. Van de Ketterij and De Pater (1997) have carried out the hydraulic fracturing experiments for the deviated well with well deviation of 49°,

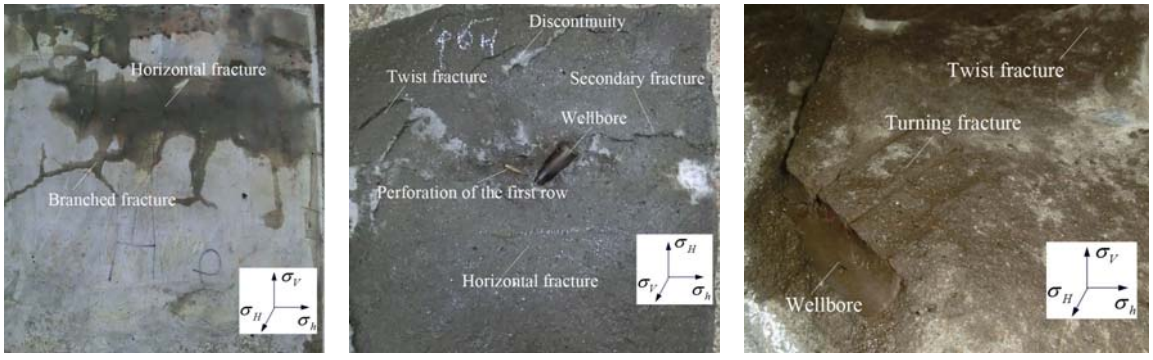

(a) 0° well azimuth (b) 45° well azimuth (c) 90° well azimuth

Fig. 9 Fracture geometries with 90° perforation angle

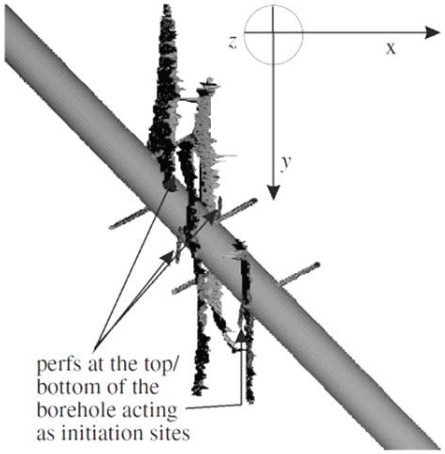

Fig. 10 There is no fractures along the tunnel when the perforation angle is 90°

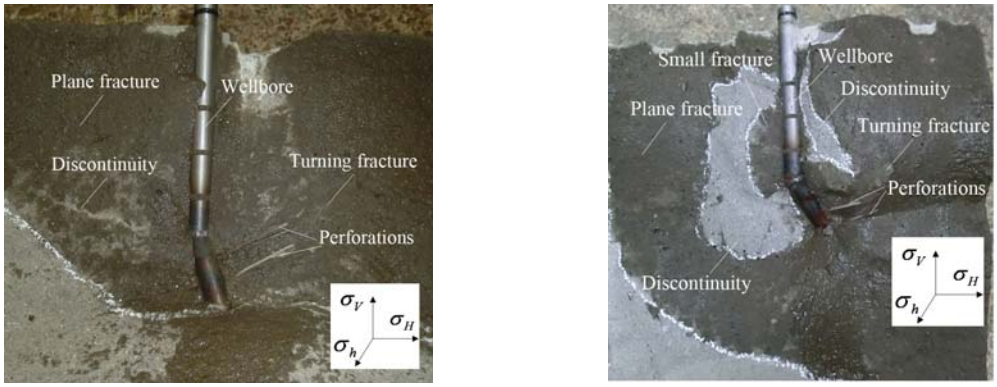

(a) 30° well deviated (b) 60° well deviated

Fig. 11 Fracture geometries with different deviated angles

well azimuth of 60° and perforation angle of 0°, 90° and 180° respectively (Fig. 10). They found that the perforation angle of 0° or 180° is the best for the fractures link-up and 90° is the worst, which are consistent with our results.

3.3 Fracture geometries with different well deviation angles

When the well azimuth and the perforation angle are both 45°, the hydraulic fracture geometries of deviated wellbores with 30°, 45° and 60° angles are studied. Fig. 11(a) illustrates that when the well deviation is 30°, the fracture initiates along the perforations and forms a turning fracture with two nearly symmetric wings; there are some discontinuous fractures. Fig. 11(b) illustrates that when the well deviation is 60°, a turning fracture is also produced at the upper side of the wellbore; although the fractures in the lower side of the wellbore initiate, they do not

propagate any further. In conclusion, when the well deviation is larger, the fracture geometrical shapes are more complicated, and the fracture initiation and propagation pressure are higher.

3.4 Fracture geometries with different well azimuths

When the well azimuth is certain, the fracture geometrical shapes become more complicated as the perforation angle increases. No matter how the well azimuth angle changes, this relationship remains the same. Under the same well azimuth angle, when the perforation angle varies from 0° to 90°, the fractures would change from the plane fracture to the turning fracture, multi-fractures and a horizontal fracture. The well azimuth has a large influence on the fracture surface roughness, the secondary fracture and the fracture continuity, but is not related to the fracture geometrical shape.

3.5 Fracture discontinuity

Hallam and Last (1991) carried out hydraulic fracturing experiments with perforating completion method for moderate deviated well. When the well deviation is less than 10°, the fracture surface is smooth no matter what the well azimuth is; when the well deviation is more than 20°, the well azimuth that produces smooth fracture surface can be expressed as

$$\tan\beta' = \frac{\left(\sin^2\beta\sin^2\alpha + \cos^2\beta\right)^{0.5}}{\sin\beta\cos\alpha} \tag{7}$$

We can find when the well deviation is 45° and well azimuth is more than 13°, the fracture is discontinuous. According to the results of this paper, when the deviation is 45° and the well azimuth is 90°, the fracture surface is still smooth. It cannot be accepted that Hallam and Last used the well deviation and well azimuth to judge whether the fracture is continuous or not. Weng (1993) used the well deviation, well azimuth, in-situ stress differentiation and the net pressure to judge whether the hydraulic fracturing could produce a continuous fracture or not, they given the following equations to calculate the critical angle that produces continuous fracture

$$\tan\phi = \tan\alpha\sin\beta \tag{8}$$

$$\tan\gamma = \sin\phi/\tan\beta \tag{9}$$

$$\sigma_\phi = \sigma_H + (\sigma_v - \sigma_H)\cos^2\phi \tag{10}$$

$$\Delta\sigma = \sigma_\phi - \sigma_h \tag{11}$$

$$\sin\gamma_{crit} = 0.57(\Delta\sigma/p_{net})^{-0.72} \tag{12}$$

Criterion for fracture links up

$$\gamma < \gamma_{crit} \tag{13}$$

The plane that contains the wellbore axis and is perpendicular to the fracture propagation

direction is called the "ϕ" plane. The angle ϕ is the angle between the "ϕ" plane and the maximum principle stress. γ is the angle between the fracture and the wellbore axis. Domain of well angles for fracture link-up of Z1-C5 well is shown in Fig. 12. When the well deviation is 45° and the well azimuth is 90°, the well angles are in the link-up area, which is consistent with the results observed by our experiments.

3.6 In-situ stress ratio on fracture geometries

The in-situ stress ratio (the maximum horizontal stress/the minimum horizontal stress) in our simulations is 1.22. According to the experiments results, the fractures include double wings fractures, turning fractures, multi-fractures, twisting fractures and horizontal fractures. Doe and Boyce (1989) carried out a laboratory hydraulic fracturing experiment on salt. They systematically studied the fracture geometrical shapes when the in-situ stress ratio varies from 1 to 2. When the stress ratio is more than 1.5, the fracture is a single plane fracture. When the stress ratio varies from 1.5 to 1, the branched fractures and multi-fractures appear, the fractures become much more

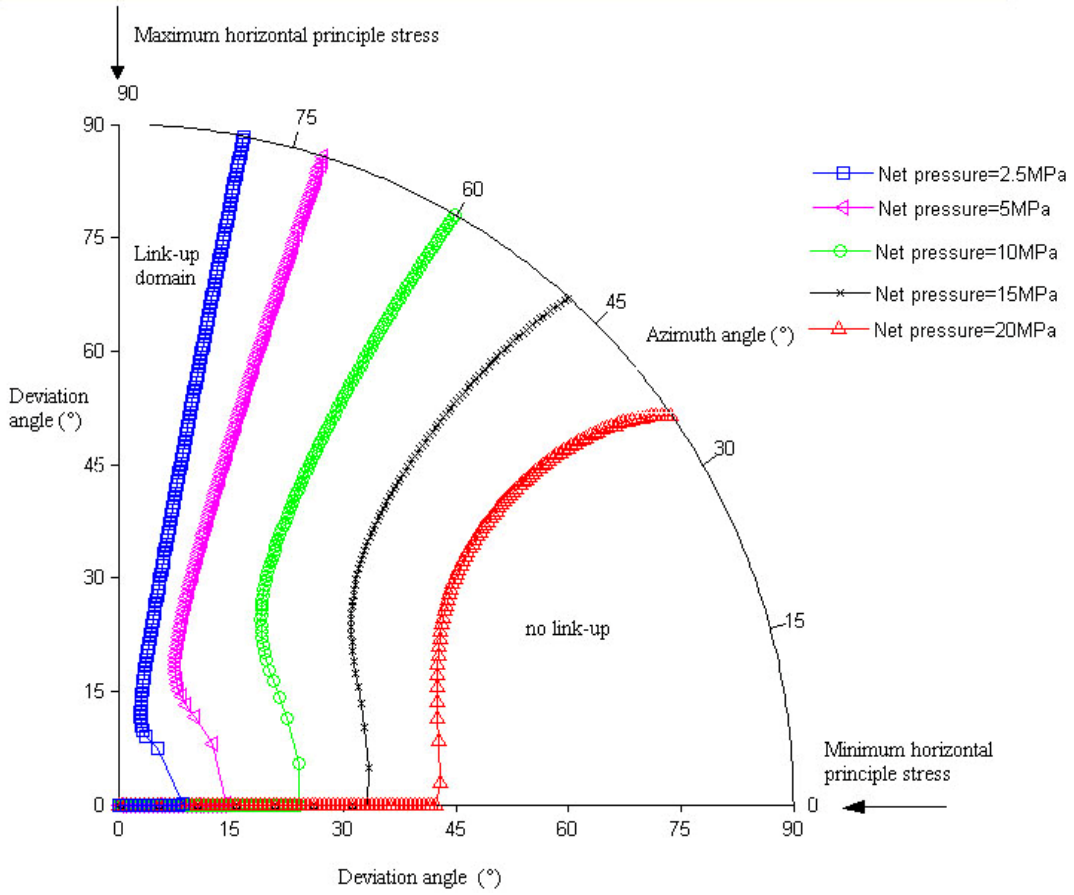

Fig. 12 Domain of well angles for fracture link-up

complicated when the ratio decreases. Beach (1980) and Daneshy *et al*. (1974) proposed the same results later. Behrmann and Elbel (1991) did the hydraulic fracturing experiments of the vertical and horizontal well under the stress ratio of 1.22, they also found the double wings fractures and multi-fractures. The results observed in our experiments of highly deviated well also show that the fractures become more complicated when the stress ratio decreases.

3.7 Perforation spacing and perforation length

In order to avoid the discontinuous fracture, Hallam and Last (1991) suggested the perforation spacing should be less than 330 mm, and the length is about 100-150 mm. Stadulis (1995) suggested that 0° perforation angle and perforation spacing within 304 mm can produce a big plane fracture. In our experiment, the perforation spacing is 200 mm and perforation length is 600 mm. No matter what the well deviation is, a plane fracture can be obtained when using the oriented perforation technique.

4. Conclusions

- When the perforation spacing is chosen as 200 mm, the perforation length is designed as 600 mm, and the perforation angle is zero in Z1-C5 well, a single plane fracture can be obtained. So these operation parameters are suggested for the hydraulic fracturing of this oilfield.
- The initiation and propagation pressure increase with the increasing of the well deviation, well azimuth and perforation angle. When the well deviation and well azimuth are certain, the perforation angle should be set as 0° (oriented perforation), so as to decrease the fracture initiation and propagation pressure.
- Whatever the well deviation and well azimuth are, when the perforation angle is 0°, a large plane fracture can be produced. When the perforation angle is not equal to 0°, the fracture geometrical shapes are very complicated. The larger the perforation angle is, the much more complicated the fracture geometrical shapes are, and the fractures are much harder to initiate from the perforations. For hydraulic fracturing of the highly deviated well, in order to obtain a big plane fracture, the orientated perforating completion technique is suggested.
- The well azimuth angle has a large influence on the roughness of the fracture surface, the creation of the secondary fractures and the fracture continuity, but has a little influence on the fracture geometrical shape. In addition, they would increase the fracture initiation and propagation pressure.

Acknowledgments

Thanks to Dr. Bao-hua Yu for proof reading and to three unknown reviewers. This work was supported by the Science Fund for Creative Research Groups of the National Natural Science Foundation of China (51221003), the National Natural Science Foundation of China (51174219) and the Key Program of National Natural Science Foundation of China (51134004). This work was supported by the National Science and Technology Major Project of the Ministry of Science and Technology of China (No. 2011ZX05024-003-02).

References

Abass, H.H. (1992), "Nonplanar fracture propagation from a horizontal wellbore: Experimental study", *SPE J.*, **11**(3), 133-137.

Abass, H.H., Brumley, J.L. and Venditto, J.J. (1994), "Oriented perforations - a rock mechanics view", *SPE Annual Technical Conference and Exhibition*, New Orleans, LA, USA, September.

Ahmed, U., Strawn, J. and Wilson, M. (1983), "Effect of stress distribution on hydraulic fracture geometry: A laboratory simulation study in one meter cubic blocks", *SPE/DOE Low Permeability Gas Reservoirs Symposium*, Denver, CO, USA, March.

Akhaveissy, A.H., Desai, C.S., Mostofinejad, D. and Vafai, A. (2013), "FE analysis of RC structures using DSC model with yield surfaces for tension and compression", *Comput. Concrete, Int. J.*, **11**(2), 123-148.

Alshoaibi, A.M. (2010), "Finite element procedures for the numerical simulation of fatigue crack propagation under mixed mode loading", *Struct. Eng. Mech., Int. J.*, **35**(3), 283-299.

Beach, A. (1980), "Numerical models of hydraulic fracturing and the interpretation of syntectonic veins", *J. Struct. Geol.*, **2**(4), 425-438.

Behrmann, L.A. and Elbel, J.L. (1991), "Effect of perforations on fracture initiation", *J. Pet. Technol.*, 5, 608-615.

Bunger, A.P., Jeffrey, R.G. and Detournay, J.E. (2005), "Application of scaling laws to laboratory-scale hydraulic fractures", *Alaska Rocks 2005, The 40th U.S. Symposium on Rock Mechanics* (*USRMS*)*: Rock Mechanics for Energy, Mineral and Infrastructure Development in the Northern Regions*, Anchorage, AL, USA, June.

Brumley, J.L. and Abass, H.H. (1996), "Hydraulic fracturing of deviated wells: Interpretation of breakdown and initial fracture opening pressure", *SPE Eastern Regional Meeting*, Columbus, OH, USA, October.

Cao, Z.J. and Liu, Y.Y. (2012), "A new numerical modelling for evaluating the stress intensity factors in 3-D fracture analysis", *Struct. Eng. Mech., Int. J.*, **43**(3), 321-336.

Chen, Z., Bunger, A.P., Zhang, X. and Jeffrey, R.G. (2009), "Cohesive zone finite element-based modeling of hydraulic fractures", *Acta Mechanica Solida Sinica*, **22**(05), 443-452.

Clifton, R.J. and Abou-Sayed, A.S. (1979), "On the computation of the three-dimensional geometry of hydraulic fractures", *Symposium on Low Permeability Gas Reservoirs*, Denver, CO, USA, May.

Daneshy, A.A. (1973a), "A study of inclined hydraulic fractures", *SPE J.*, **13**(2), 61-68.

Daneshy, A.A. (1973b), "Experimental investigation of hydraulic fracturing through perforations", *The 5th Annual Offshore Technology Conference*, Houston, TX, USA, April.

Daneshy, A.A. (1974), "Hydraulic fracture propagation in the presence of planes of weakness", *SPE European Spring Meeting*, Amsterdam, Netherlands, May.

De Pater, C.J., Cleary, M.P., Quinn, T.S., Barr, D.T., Johnson, D.E. and Weijers, L. (1994), "Experimental verification of dimensional analysis for hydraulic fracturing", *SPE Prod. Facil.*, **4**, 230-238.

Deng, J.G., Guo, X.M., Sun, Y., Qi, B. and Lei, W. (2008), "Research on oriented perforation optimization technique for fracturing wells in tight gas reservoir" *Oil Drill. Prod. Tech.*, 6, 93-96. [In Chinese]

Doe, T.W. and Boyce, G. (1989), "Orientation of hydraulic fractures in salt under hydrostatic and non-hydrostatic stresses", *Int. J. Rock Mech. Min. Sci. Geomech. Abstr.*, **26**(6), 605-605.

EI Rabaa, W. (1989), "Experimental study of hydraulic fracture geometry initiated from horizontal wells", *SPE Annual Technical Conference and Exhibition*, San Antonio, TX, USA, October.

Hallam, S.D. and Last, N.C. (1991), "Geometry of hydraulic fractures from modestly deviated wellbore", *J. Pet. Technol.*, **43**(6), 742-748 .

Hossain, M.M. and Rahman, M.K. (2008), "Numerical simulation of complex fracture growth during tight reservoir stimulation by hydraulic fracturing", *J. Petrol. Sci. Eng.*, **60**(2), 86-104.

Kim, C.M. and Abass, H.H. (1991), "Hydraulic fracture initiation from horizontal wellbores: Laboratory experiments", *Rock Mech. as a Multidiscip. Sci.*, Balkema, Rotterdam, Roegiers, July.

Kim, W.-J., Lee, J.-M., Kim, J.-S. and Lee C.J. (2012), "Measuring high speed crack propagation in concrete fracture test using mechanoluminescent material", *Smart Struct. Syst., Int. J.*, **10**(6), 547-555.

King, G.E. (1989), "Perforating the horizontal well", *J. Pet. Technol.*, **7**, 671-672.

Khristianovic, S.A. and Zheltov, Y.P. (1955), "Formation of vertical fractures by means of highly viscous liquid", *Proceedings of the 4th World Petroleum Congress*, Rome, Italy, June.
Liao, F., Wang, W. and Chen. Y. (2012), "Parameter calibrations and application of micromechanical fracture models of structural steels", *Struct. Eng. Mech., Int. J.*, **42**(2),153-174.
Liu, G.H., Pang, F. and Chen, Z.X. (2000), "Development of scaling laws for hydraulic fracture simulation tests", *J. Univ. Petrol., China* (*Edition of Natural Science*), **5**, 45-48. [In Chinese]
Luo, X., Ge, H. and Ohashi, M. (2012), "Experimental study on ductile crack initiation in compact section steel columns", *Steel Compos. Struct., Int. J.*, **13**(4), 383-396.
Mack, M.G. and Warpinski, N.R. (2000), "Mechanics of hydraulic fracturing", (*Economides, N. Eds.*, 3rd Edition), *Reservoir Stimulation*, Chichester, Wiley.
Mahrer, K.D., Aud, W.W. and Hansen, J.T. (1996), "Far-field hydraulic fracture geometry: A changing paradigm", *SPE Annual Technical Conference and Exhibition*, Denver, CO, USA, October.
Nagel, N.B. and Sanchez-Nagel, M. (2011), "Stress shadowing and microseismic events: A numerical evaluation", *SPE Annual Technical Conference and Exhibition*, Denver, CO, USA.
Nagel, N.B., Sanchez-Nagel, M. and Lee, B. (2012), "Gas shale hydraulic fracturing: A numerical evaluation of the effect of geomechanical parameters", *SPE Hydraulic Fracturing Technology Conference*, The Woodlands, TX, USA.
Nordgren, R.P. (1972), "Propagation of a vertical hydraulic fracture", *SPE J.*, **4**, 306-314.
Pearson, C.M., Bond, A.J., Eck, M.E. and Schmldt, J.H. (1992), "Results of stress oriented and aligned perforating in fracturing deviated wells", *J. Pet. Technol.*, **44**(1), 10-18.
Pollard, D.D., Segall, P. and Delaney, P.T. (1982), "Formation and interpretation of dilatant echelon cracks", *Geol. Soc. Am. Bull.*, **93**(12), 1291-1303.
Rahman, M.M., Hossain, M.M., Crosby, D.G., Rahman, M.K. and Rahman, S.S. (2002), "Analytical, numerical and experimental investigations of transverse fracture propagation from horizontal wells", *J. Petrol. Sci. Eng.*, **35**(3-4), 127-150.
Siebrits, E. and Peirce, A.P. (2002), "An efficient multi-layer planar 3D fracture growth algorithm using a fixed mesh approach", *Int. J. Numer. Meth. Eng.*, **53**(3), 691-717.
Sneddon, I.N. and Elliott, H.A. (1946), "The opening of a Griffith crack under internal pressure", *Q. Appl. Math.*, **3**, 262-267.
Soliman, M.Y., East, L. and Adams, D. (2008), "Geomechanics aspects of multiple fracturing of horizontal and vertical wells", *SPE Drill. Completion*, **23**(3), 217-228.
Stadulis, J.M. (1995), "Development of a completion design to control screenouts caused by multiple near-wellbore fractures", *SPE Rocky Mountain Regional / Low Permeability Reservoirs Symposium*, Denver, CO, USA, March.
Tada, H., Paris, P.C. and Irwin, G.R. (1985), "The stress analysis of cracks handbook", Louis, MO, USA.
Tang, C.A., Tham, L.G., Lee, P.K.K., Yanga, T.H. and Lia, L.C. (2002), "Coupling analysis of flow, stress and damage (FSD) in rock failure", *Int. J. Rock Mech. Min. Sci.*, **39**(4), 477-489.
van de Ketterij, R.G., de Pater, C.J. (1997), "Experimental study on the impact of perforations on hydraulic fracturing tortuosity", *SPE European Formation Damage Conference*, Hague, The Netherlands, June.
Weijers, L. and De Pater, C.J. (1992), "Facture reorientation in model tests", *SPE Formation Damage Control Symposium*, Lafayette, LA, USA, February.
Weng, X.W. (1993), "Fracture initiation and propagation from deviated wellbores", *SPE Annual Technical Conference and Exhibition*, Houston, TX, USA, October.
Zhang, G.M., Liu, H., Zhang, J., Wu, H.A. and Wang, X.X. (2010), "Three-dimensional finite element simulation and parametric study for horizontal well hydraulic fracture", *J. Petrol. Sci. Eng.*, **72**(3-4), 310-317.
Zhang, G.Q., Chen, M. and Zhao Y.B. (2008), "Study on initiation and propagation mechanism of fracturesin oriented perforation of new wells", *Acta petrol ei sinica*, **29**(1), 117-119. [In Chinese]
Zhang, X, Jeffrey, R.G. and Thiercelin, M. (2007), "Deflection and propagation of fluid-driven fractures at frictional bedding interfaces: A numerical investigation", *J. Struct. Geol.*, **29**(3), 396-410.
Zhang, X., Jeffrey, R.G. and Thiercelin, M. (2009), "Mechanics of fluid-driven fracture growth in naturally

fractured reservoirs with simple network geometries", *J. Geophys. Res. – Sol d Earth*, **114**(B12), 402-406.
Zhou, J., Jin, Y. and Chen, M. (2010), "Experimental investigation of hydraulic fracturing in random naturally fractured blocks", *Int. J. Rock Mech. Min. Sci*., **47**, 1193-1199.
Zhu, X.H., Liu, S.H., Tong, H. and Liu, Y.H. (2012), "Experimental and numerical study of drill pipe erosion wear in gas drilling", *Eng. Fail. Anal*., **26**, 370-380.
Zhu, H.Y., Deng, J.G., Li, S.Y., Chen, Z.J., Yan, W., Hu, L.B., Lin, H. and Yan, C.L. (2013), "Numerical simulation and laboratory experiments of hydraulic fracturing of highly deviated well", *Applied Mechanics and Materials*, **275-277**, 278-281.
Zhu, H.Y., Deng, J.G., Xie, Y.H., Huang, K.W., Zhao, J.Y. and Yu, B.H. (2012), "Rock mechanics characteristic of complex formation and faster drilling techniques in Western South China Sea oilfields", *Ocean Eng*., **44**, 33-45.

PL

Appendix

The governing equations of Clifton and Abou-Sayed (1979) include equilibrium equation, continuity equation and pressure gradient equation, which are listed as follows

$$\begin{cases} \Delta p(x,y) = p(x,y) - \sigma_{zz}^{0}(x,y,0) = Ee\iint\limits_{A}\left\{\dfrac{\partial}{\partial x}\left[\dfrac{1}{R}\dfrac{\partial w(x,y)}{\partial x}\right] + \dfrac{\partial}{\partial y}\left[\dfrac{1}{R}\dfrac{\partial w(x,y)}{\partial y}\right]\right\}dxdy \\ \dfrac{\partial q_x}{\partial x} + \dfrac{\partial q_y}{\partial y} + \dfrac{\partial w}{\partial t} + \dfrac{2K_L\dfrac{p_i - p_0}{\sigma_{zz}^{0}(0,0) - p_0}}{\sqrt{t-\tau(x,y)}} - q_1 = 0 \\ \dfrac{\partial p}{\partial x} + \eta\dfrac{q_x}{w^3} = 0 \\ \dfrac{\partial p}{\partial y} + \eta\dfrac{q_y}{w^3} = \rho F_y \\ R = [(x-x_0)^2 + (y-y_0)^2]^{1/2} \end{cases} \tag{A.1}$$

where, Ee is the equivalent elastic modulus, p_i is the fluid pressure inside the fracture, σ_{zz}^{0} is the normal pressure of fracture surface before hydraulic fracturing, K_L is the total leak-off coefficient, η is the viscosity coefficient of hydraulic fracturing fluid, R is the distance between integral point (x, y) of integrand and the pressure point (x_0, y_0), w is the fracture width, q_x is the volume flow rate per unit length along x direction, q_y is the volume flow rate per unit length along y direction, q_1 is the injection rate per unit area of the fracture, τ is the contact time between the fracture and frac fluid, T is the fracture propagation time, Q is the hydraulic fracturing pumping flow, ρ the density of the hydraulic fracturing fluid.

Fracture propagation condition

$$w_a(s) > w_c = \frac{K_{1c}}{2\pi Ee}\left[\frac{2a(s)}{\pi}\right]^{1/2} \tag{A.2}$$

where, a is the width of vicinity area of the fracture end point, K_{1c} is the critical stress intensity factor of fracture propagation, w_c the critical fracture width of fracture propagation. When $w_a(s) < w_c$, fracture propagation terminates. According to the similarity principle, nine single boundary value conditions are given

$$\frac{p_0}{Ee_0}=1;\frac{\sigma_0}{Ee_0}=1;\frac{l_0^2}{t_0 q_0}=1;\frac{t_0 K_{L0}}{q_0\sqrt{t_0}}=1;\frac{q_{10}l_0}{q_0}=1;\frac{q_0\eta_0}{p_0 l_0^2}=1;\frac{l_0\rho F_{y0}}{p_0}=1;\frac{K_{IC0}}{Ee_0\sqrt{L_0}}=1;\frac{Q_0}{q_0 l_0}=1 \tag{A.3}$$

Dimensionless form of the Eqs. (A.1) and (A.2)

$$\begin{cases} \overline{p}^{(k)} - \overline{\sigma}_{zz}^{0(k)} = \iint\limits_{\overline{A}} \left\{ \dfrac{\partial}{\partial \overline{x}} \left[\dfrac{1}{\overline{R}} \dfrac{\partial \overline{w}}{\partial \overline{x}} \right] + \dfrac{\partial}{\partial \overline{y}} \left[\dfrac{1}{\overline{R}} \dfrac{\partial \overline{w}}{\partial \overline{y}} \right] \right\} d\overline{x} d\overline{y} \\ \dfrac{\partial \overline{q}_x^{(k)}}{\partial \overline{x}} + \dfrac{\partial \overline{q}_y^{(k)}}{\partial \overline{y}} + \dfrac{\partial \overline{w}}{\partial \overline{t}^{(-k)}} + \dfrac{2\overline{K}_L^{(k)} \dfrac{\overline{p}_i^{(k)} - \overline{p}_0^{(k)}}{\overline{\sigma}_{zz}^{0(k)} - \overline{p}_f^{(k)}}}{\sqrt{\overline{t}^{(k)} - \overline{\tau}^{(k)}}} - \overline{q}_1^{(k)} = 0 \\ \dfrac{\partial \overline{p}^{(k)}}{\partial \overline{x}} + \overline{\eta}^{(k)} \dfrac{\overline{q}_x^{(k)}}{\overline{w}^3} = 0 \\ \dfrac{\partial \overline{p}^{(k)}}{\partial \overline{y}} + \overline{\eta}^{(k)} \dfrac{\overline{q}_y^{(k)}}{\overline{w}^3} = \overline{\rho F_y}^{(k)} \\ \overline{w}_c = \dfrac{\overline{K}_{1C}^{(k)}}{2\pi} \left[\dfrac{2\overline{a}}{\pi} \right]^{1/2} \\ 1 = 2\int_{-\overline{h}/2}^{\overline{h}/2} \overline{q}_x^{(k)}(0, \overline{y}, \overline{t}^{(k)}) d\overline{y} \\ \overline{t}^{(k)} = \overline{T}^{(k)} \\ \overline{x}_{\max} = 1 \end{cases} \tag{A.4}$$

where the dimensionless is

$$\begin{cases} \overline{L} = 1, \overline{E}_e = 1, \overline{Q} = 1, \overline{x} = \dfrac{x}{L}, \overline{y} = \dfrac{y}{L} \\ \overline{w} = \dfrac{w}{L}, \overline{w}_c = \dfrac{w_c}{L}, \overline{R} = \dfrac{R}{L}, \overline{h} = \dfrac{h}{L}, \overline{a} = \dfrac{a}{L}, \overline{p}^{(k)} = \dfrac{p_i}{Ee} \\ \overline{p}_f^{(k)} = \dfrac{p_0}{Ee}, \overline{\sigma}_{zz}^{0(k)} = \dfrac{\sigma_{zz}^0}{Ee}, \overline{\rho F y}^{(k)} = \dfrac{\rho F y L}{Ee}, \overline{q}_1^{(k)} = \dfrac{q_1 L^2}{Q} \\ \overline{q}_x^{(k)} = \dfrac{q_x L}{Q}, \overline{q}_y^{(k)} = \dfrac{q_y L}{Q}, \overline{\eta}^{(k)} = \dfrac{\eta Q}{EeL^3}, \overline{t}^{(k)} = \overline{\tau}^{(k)} = \dfrac{\tau Q}{L^3} \\ \overline{K}_L^{(k)} = \dfrac{K_L}{K_{L0}^{(k)}} = K_L \sqrt{\dfrac{L}{Q}}, \overline{K}_{IC}^{(k)} = \dfrac{K_{IC}}{K_{IC0}^{(k)}} = \dfrac{K_{IC}}{Ee\sqrt{L}} \end{cases} \tag{A.5}$$

where L is the length. Substituting the single-value condition (A.3) into dimensionless equation (A.5), we have the dimensionless similarity principle

$$\frac{p_i}{Ee} = A; \frac{p_0}{Ee} = A; \frac{\sigma_{zz}^0}{Ee} = A; \frac{L\rho F_y}{Ee} = A; \frac{TQ}{L^3} = A; K_L \sqrt{\frac{L}{Q}} = A; \frac{K_{IC}}{Ee\sqrt{L}} = A; \frac{\eta Q}{EeL^3} = A \tag{A.6}$$

where, A is constant. After simplifying (A.6), we obtain the dimensionless similarity index

$$\frac{C_{p_i}}{C_{Ee}} = \frac{C_{\sigma_{zz}^0}}{C_{Ee}} = \frac{C_T C_Q}{C_L^3} = C_{K_L}\sqrt{\frac{C_L}{C_Q}} = \frac{C_{K_{IC}}}{C_{Ee}\sqrt{C_L}} = \frac{C_\eta C_Q}{C_{Ee} C_L^{\ 3}} = B = \text{constant} \tag{A.7}$$

where, the similarity principle is

$$C_V = V_{\text{model}} / V_{field} \tag{A.8}$$

where, $V = L$, Ee, Q, T, K_L, η, p_i, σ_{ZZ}^0, K_{IC}, C_V is the ratio of the model quantities to the prototype quantities.